Impact of atomic reconstruction on optical spectra of twisted TMD homobilayers

Impact of atomic reconstruction on optical spectra of twisted TMD homobilayers

Joakim Hagel,[1,*] Samuel Brem,[2] Johannes Abelardo Pineiro,[2] and Ermin Malic[2,1]
[1]*Department of Physics, Chalmers University of Technology, 412 96 Gothenburg, Sweden*
[2]*Department of Physics, Philipps University of Marburg, 35037 Marburg, Germany*

(Received 29 August 2023; revised 8 December 2023; accepted 12 February 2024; published 4 March 2024)

Twisted bilayers of transition metal dichalcogenides (TMDs) have revealed a rich exciton landscape including hybrid excitons and spatially trapped moiré excitons that dominate the optical response of the material. Recent studies have shown that in the low-twist-angle regime, the lattice undergoes a significant relaxation in order to minimize local stacking energies. Here, large domains of low energy stacking configurations emerge, deforming the crystal lattices via strain and consequently impacting the electronic band structure. However, so far the direct impact of atomic reconstruction on the exciton energy landscape and the optical properties has not been well understood. Here, we apply a microscopic and material-specific approach and predict a significant change in the potential depth for moiré excitons in a reconstructed lattice, with the most drastic change occurring in naturally stacked TMD homobilayers. We show the appearance of multiple flat bands and a significant change in the position of trapping sites compared to the rigid lattice. Most importantly, we predict a multipeak structure emerging in optical absorption of WSe_2 homobilayers—in contrast to the single peak that dominates the rigid lattice. This finding can be exploited as an unambiguous signature of atomic reconstruction in optical spectra of moiré excitons in naturally stacked twisted homobilayers.

DOI: 10.1103/PhysRevMaterials.8.034001

I. INTRODUCTION

The recent advances in the field of two-dimensional materials have opened up a new platform to study many-particle physics in nanomaterials [1]. The field of twistronics is of particular interest, where the relative twist angle between two vertically stacked 2D materials can be used as an additional external knob to tune the material properties [2–4]. Consequently, the introduction of a twist angle in these layered systems can lead to intriguing many-particle phenomena, such as unconventional superconductivity and correlated phases [5,6]. Transition metal dichalcogenides (TMDs) have emerged as a significant and noteworthy subclass of two-dimensional materials, garnering substantial interest in recent years [7,8]. Here, strongly bound electron-hole pairs, known as excitons, form due to the two-dimensional confinement and the reduced screening of the Coulomb interaction. They dominate the material's optical response even at room temperature [9–12]. Furthermore, long-lived interlayer excitons can form, which exhibit an out-of-plane dipole moment due to the spatial separation of electrons and holes [13–20]. Additionally, the large wave function overlap can lead to a significant carrier tunneling between the layers, giving rise to hybrid states of intra and interlayer excitons [10,19,21–24].

When introducing a twist angle between two vertically stacked TMDs, a periodic superlattice emerges. This leads to a moiré pattern, i.e., a periodic superlattice potential that can trap excitons at specific high-symmetry sites [21,25–31]. Furthermore, the emerging moiré potential can be tuned by changing the twist angle which has been shown to have a large impact on the optical response of these materials [25,26,29,32–34]. Interestingly, recent studies have revealed that when the twist angle is small, i.e., the period of the moiré pattern is large, the two monolayer crystal lattices no longer remain rigid, but instead undergo a deformation to reduce the total adhesion energy [35–43]. Here, some energetically favorable high-symmetry sites grow to form large domains, separated by typically narrow domain walls (cf. Fig. 1). It has been predicted that this atomic reconstruction should have a major impact on the electronic band structure and fundamentally change the potential landscape [38,44–47]. However, it is still not thoroughly understood how atomic reconstruction can be identified in the optical response of moiré excitons.

In this work, we investigate photoluminescence (PL) and absorption spectra in atomically reconstructed TMD bilayers. Our approach is based on the *ab initio* derived continuum model for the deformation of the rigid lattice derived in Refs. [45,46] combined with an equation-of-motion approach for the optical response of moiré excitons [19,21,30,31]. This allows us to obtain microscopic insights into the changes in the moiré exciton energy landscape and the optical response in the presence of atomic reconstruction. The deformation of the moiré supercell into large periodic domains induces strain that can result in deeper potentials for moiré excitons. As a direct

*joakim.hagel@chalmers.se

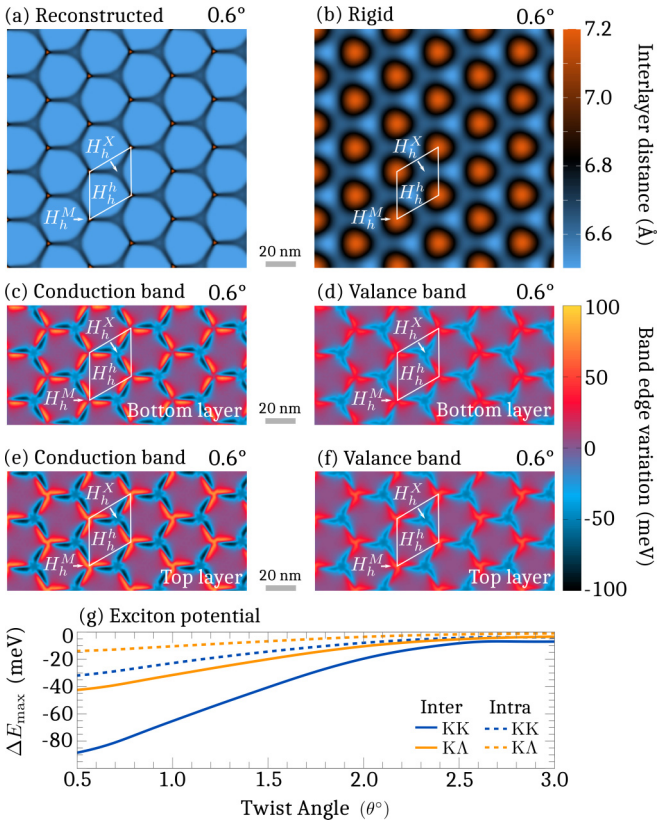

FIG. 1. Spatial map of the interlayer distance in (a) a reconstructed lattice and (b) a rigid lattice at $\theta = 0.6^\circ$ for H-type stacked WSe_2 homobilayers. Here, the interlayer distance is associated with a high-symmetry stacking. The band edge variation for the conduction band in (c) the bottom layer and (e) the top layer at the K point, and the valance band edge variation in (d) the bottom layer and (f) the top layer at the K point. Note the reversed sign between the layers and the difference in the potential depth between valance and conduction band. Since this is a purely strain-induced potential, it is not present in the rigid lattice. The shape of the potential stems from the linear combination of the scalar strain potential and the piezo potential. (g) Maximum exciton potential depth ΔE_{max} in the supercell is shown as a function of twist angle for both intralayer excitons (dashed) and interlayer excitons (solid).

consequence, we find more trapped states than in the rigid lattice and the stacking region in which excitons are trapped can differ from the rigid lattice system. Furthermore, we predict that the KK interlayer exciton becomes lower in energy than the intralayer KK state due to the strain-induced potentials at low twist angles. The lowest lying momentum-dark KΛ exciton is also predicted to undergo a larger red shift than in the rigid lattice, visible in PL spectra. Most importantly, we find a qualitative change in the absorption spectrum in naturally stacked bilayers reflecting the bright KK excitons, where multiple peaks emerge as a consequence of the strain-induced potentials—in stark contrast to the single peak that is present in the rigid lattice. Consequently, we predict an unambiguous signature of atomic reconstruction in the optical response of moiré excitons in naturally stacked twisted TMD homobilayers.

II. MOIRÉ POTENTIAL IN ATOMICALLY RECONSTRUCTED TMD BILAYERS

To gain access to the moiré exciton energy landscape in atomically reconstructed bilayers, we first describe the change in geometry in the superlattice. Following the approach in Refs. [45,46] we set up a functional for the stacking energy, taking into account the strain energy from continuum theory and a parametrized equation for the adhesion energy between the layers, where the model parameters have been fitted to data from density functional theory in Refs. [45,47]. The functional can then be turned into an optimization problem by expanding the displacement vectors $\mathbf{u}^l(\mathbf{r})$ as a Fourier expansion $\mathbf{u}^l(\mathbf{r}) = \sum_n \mathbf{u}^l_n e^{i\mathbf{g}_n\mathbf{r}}$ and minimizing the integral with respect to the Fourier coefficients $\mathbf{u}^l_n$. Here, l is the layer index, $\mathbf{g}_n$ are the reciprocal vectors of the moiré lattice and $\mathbf{r}$ is the real space coordinate in the supercell. For further details, see the Supplemental Material (SM) of the paper [48] (see also Refs. [49–57] therein).

After obtaining the displacement vectors, we study the geometrical change in the supercell. Here, we find that the energetically more favorable H^h_h stacking grows into hexagonal domains (Kagome pattern) at small twist angles, separated by a thin boundary wall—in good agreement with experimental studies [35] and previous theoretical works [45]. This reconstruction is illustrated in Fig. 1(a), showing the interlayer distance for H-type stacked WSe_2 homobilayers at the twist angle $\theta = 0.6^\circ$. Each high-symmetry stacking is reflected by a specific interlayer distance, which can be computed from DFT [58] and thus, the interlayer distance can be used as an indicator for a change in the local atomic registry. The blue domains denote the H^h_h regions, which are significantly larger than in the rigid lattice, cf. Fig. 1(b). The other high-symmetry stackings (H^X_h and H^M_h) consequently shrink in size and form thin boundary networks [cf. Fig. 1(a)]. We focus here on the examplary H-type stacked WSe_2 homobilayer, but the same approach holds for all vertically stacked TMDs. In R-type stacked homobilayers, we instead obtain large triangular patterns as a result of the atomic reconstruction, which yields a different potential landscape (see the SM [48] for further details).

The impact of atomic reconstruction on the exciton energy landscape does not only stem from the geometrical change in the superlattice, but also from the strain that accompanies the lattice deformation. Assuming small displacements, the displacement vector $\mathbf{u}^l(\mathbf{r})$ can be associated to the linear strain tensor $\varepsilon_{ij} = \frac{1}{2}(u_{i,j} + u_{j,i})$, where $u_{i,j} = \frac{1}{2}(\partial_i u_j + \partial_j u_i)$ and $i(j) = (x, y)$. Due to its D3h symmetry, we can decompose the dominating strain contributions to the moiré potential into two parts (see the SM [48]) [59–61]: scalar potential composed of inhomogeneous uniaxial strain in both the x and y directions [62,63] and inhomogeneous vector gauge potential known as piezo potential [45,47,64]. Details about the strain potential model are provided in the SM [48].

In addition to the strain-induced potentials, there is a stacking-dependent alignment shift of the two monolayer band structures, originating from charge polarization between the two layers, that already exists in the nonreconstructed system [19,30]. In a homobilayer, these only affect the energy of interlayer excitons [19]. Furthermore, it is only present in

R-type stacked bilayers due to the lack of inversion symmetry, which allows for local charge transfers between the layers [27]. The remaining interlayer coupling mechanism contributing to the total moiré potential is given by the interlayer hybridization. For some electronic states, in particular in the Λ valley in the conduction band, the large wave function overlap between the layers leads to a strong mixing of states in both layers, which can be described as a mixing of interlayer and intralayer excitons into hybrid exciton states [19,21]. In H-type stacking, the strongest hybridization occurs around the H_h^h stacking due to its shorter interlayer distance cf. Figs. 1(a) and 1(b). To sum up, we have four different contributions to the moiré potential: (i) scalar strain potential $S^{\xi}_{L\mathbf{g}}$, (ii) piezo potential $P^{\xi}_{L\mathbf{g}}$, (iii) stacking-dependent alignment potential $V^{\xi}_{L\mathbf{g}}$, and (iv) tunneling $T^{\xi}_{LL'\mathbf{g}}$. The first three act as a periodic renormalization of exciton energies, i.e., they are diagonal with respect to the layer index, and can thus be modeled as an external potential acting on free excitons $M^{\xi}_{L\mathbf{g}} = S^{\xi}_{L\mathbf{g}} + P^{\xi}_{L\mathbf{g}} + V^{\xi}_{L\mathbf{g}}$, where $L = (l_e, l_h)$ is a compound layer index and $\xi = (\xi_e, \xi_h)$ is the exciton valley index.

In Figs. 1(c) and 1(d), we show the resulting band edge variation for the conduction band [Fig. 1(c)] and the valance band [Fig. 1(d)] in the bottom layer at $\theta = 0.6^\circ$. Similarly, the band edge variation for the top layer is shown in Figs. 1(e) and 1(f), where the conduction band is given by Fig. 1(e) and the valance band is given by Fig. 1(e) at $\theta = 0.6^\circ$. Here, the only potentials that are contributing are the scalar strain potential and the piezo potential. In general, homobilayers mostly reconstruct due to atomic rotation [37], which is associated with the piezo potential and will be concentrated at the H_h^M/H_h^X sites. However, there is also a significant scalar strain potential close to the boundary regions of the H_h^h domains which also significantly contribute to the band edge variation. The combination of scalar potential and piezo potential in turn gives the tilted star-shape of the total band edge variation. Comparing the variation for different layers [Figs. 1(e)-1(d)] we find that the minima of the conduction band and the maxima of the valance band occur at the same sites, thus yielding a very efficient band gap renormalization for interlayer excitons. In contrast, comparing Figs. 1(c) and 1(d) we find that the minima for the conduction band and the maxima for the valance band occur at different sites in the supercell. This means that there is a certain driving force for charge separation. However, the binding energies of the intralayer excitons are very strong (~ -140 meV for KK) which in turn means that one would need a very deep potential in order to have a complete charge separation. At angles $\theta > 0.5^\circ$, the formation of excitons is still favored in comparison to the separated unbounded electron/holes. For much smaller supercells, however, the formation of in-plane charge transfer excitons can occur as reported in [38].

The effective exciton potential as shown in Fig. 1(g) gives the calculated potential depth for KK (blue) and KΛ (yellow) excitons as a function of twist angle, both for intra (dashed) and interlayer (solid) excitons. Since the piezo potential in H-type stacking is the same for both the valence and the conduction band in both layers, the only contributing factor is the scalar strain potential. The color map of this effective potential is given in the Supplemental Material. Below $\theta = 2^\circ$ we find a significant decrease of the KK interlayer exciton potential (solid blue) due to the efficient band gap renormalization stemming from the scalar strain potential. The KK intralayer (dashed blue) potential has a much shallower potential due to the conduction and valance band shifting in the same direction, although with different rates. Comparing to the effective KΛ (solid yellow) potential, it only reaches half the potential depth of the KK. This can be understood from different orbital compositions of the valleys, which directly impact the change in the orbital overlap with scalar strain [65]. Note that these effective exciton potentials are all in stark contrast to the rigid lattice where they do not occur at all for H-type stacking. For R-type stacking, we predict in general much weaker band edge variations, having only a maximum variation of ∼40 meV. This difference comes primarily from the lack of scalar strain in R-type stacking, where the domain walls are formed purely from shear strain—in good qualitative agreement with the experimentally observed values [37]. In turn, this means that the effective intralayer exciton potential will be close to 0 meV. There will, however, be a significant addition to the interlayer potential in the form of the piezo potential (see the SM [48]).

III. MOIRÉ EXCITON ENERGY LANDSCAPE IN RECONSTRUCTED TMD BILAYERS

Having microscopic access to the potential landscape of moiré excitons, we can now set up the complete moiré exciton Hamilton operator. Here, we start from a decoupled monolayer basis in electron-hole picture and add the moiré potential as periodic modifications to these energies [21,30,31]. Transforming to an exciton basis, the Hamiltonian then reads

$$H_0 = \sum_{L\mathbf{Q}\xi} E^{\xi}_{L\mathbf{Q}} X^{\xi\dagger}_{L\mathbf{Q}} X^{\xi}_{L\mathbf{Q}} + \sum_{L\mathbf{Q}\xi\mathbf{g}} M^{\xi}_{L\mathbf{g}} X^{\xi\dagger}_{L\mathbf{Q}+\mathbf{g}} X^{\xi}_{L\mathbf{Q}} + \sum_{LL'\mathbf{Q}\xi\mathbf{g}} T^{\xi}_{LL'\mathbf{g}} X^{\xi\dagger}_{L\mathbf{Q}+\mathbf{g}} X^{\xi}_{L'\mathbf{Q}} + \text{H.c.}, \quad (1)$$

where $E^{\xi}_{L\mathbf{Q}}$ is the binding energy of the decoupled monolayer as obtained from the generalized Wannier equation [66] and $\mathbf{Q}$ is the center-of-mass momentum. The effective masses for electrons and holes are obtained from Ref. [67]. Furthermore, $X^{(\dagger)}$ denotes the annihilation (creation) operator of excitons. Moreover, $M^{\xi}_{L\mathbf{g}}$ is the combined layer-diagonal moiré potential component and $T^{\xi}_{LL'\mathbf{g}}$ is the tunneling matrix element. The latter gives rise to the hybridization of intra and interlayer excitons, which corresponds to the off-diagonal component of the moiré potential [58].

The periodicity of the superlattice is taken into account by applying the zone-folding scheme [21,30,31], where we restrict the summation over $\mathbf{Q}$ to the first mini-Brillouin zone (mBZ), where states with larger momentum are folded back via mBZ lattice vectors $\mathbf{g}$ giving rise to the formation of mini subbands. The final moiré exciton energies are then obtained by first expanding the exciton operators into a moiré exciton basis $Y^{\dagger}_{\xi\eta\mathbf{Q}} = \sum_{\mathbf{g}L} \mathcal{C}^{\xi\eta*}_{L\mathbf{g}}(\mathbf{Q}) X^{\xi\dagger}_{L,\mathbf{Q}+\mathbf{g}}$, where $Y^{(\dagger)}$ are the moiré exciton annihilation (creation) operators, η is the new band index, and $\mathcal{C}^{\xi\eta*}_{L\mathbf{g}}(\mathbf{Q})$ are the mixing coefficients that mix different subbands and layer configurations. Applying this

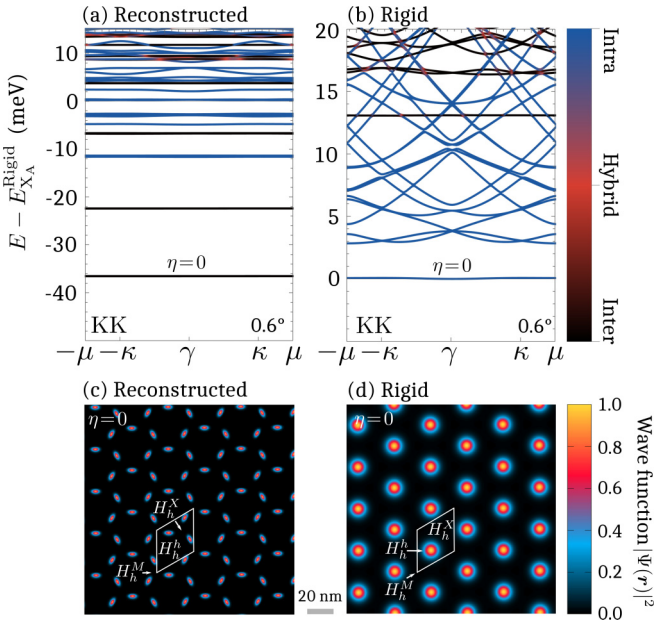

FIG. 2. Band structure and wave function of the bright KK exciton in H-type stacked WSe_2 bilayer at $\theta = 0.6^\circ$ in (a), (c) the reconstructed lattice and (b), (d) the rigid lattice. Energies are normalized to the lowest-lying KK exciton in the rigid lattice. Note that the reconstruction drastically changes the localization site of excitons and that the efficient moiré potential for interlayer excitons shifts them below the intralayer KK states. The band index $\eta = 0$ indicates which wave function is shown.

transformation to Eq. (1) we obtain the moiré exciton eigenvalue equation

$$E^{\xi}_{L\mathbf{Q}+\mathbf{g}} C^{\xi\eta}_{L\mathbf{g}}(\mathbf{Q}) + \sum_{\mathbf{g}'} M^{\xi}_{L}(\mathbf{g},\mathbf{g}') C^{\xi\eta}_{L\mathbf{g}'}(\mathbf{Q}) + \sum_{L'\mathbf{g}'} T^{\xi}_{LL'}(\mathbf{g},\mathbf{g}') C^{\xi\eta}_{L'\mathbf{g}'}(\mathbf{Q}) = \mathcal{E}^{\xi}_{\eta\mathbf{Q}} C^{\xi\eta}_{L\mathbf{g}}(\mathbf{Q}). \quad (2)$$

Here, $\mathcal{E}^{\xi}_{\eta\mathbf{Q}}$ are the final moiré exciton energies, which can be obtained by solving Eq. (2) numerically.

In Fig. 2, we show the calculated moiré exciton band structure for H-type stacked hBN-encapsulated WSe_2 bilayers (for R-type stacking, see the SM [48]) with a reconstructed lattice [Fig. 2(a)] and with a rigid lattice [Fig. 2(b)]. We find a large redshift in the reconstructed lattice, where the lowest subband is located ∼36 meV below the rigid lattice energies. Interestingly, due to the efficient moiré potential for the interlayer exciton, the nature of the lowest lying state has changed from an intralayer exciton to an interlayer exciton. While in the rigid lattice [cf. Fig. 2(b)] most bands have a significant curvature, we find multiple ultraflat bands in the reconstructed lattice [cf. Fig. 2(a)], both for the interlayer excitons (black) and the intralayer excitons (blue). The spacing between the first two bands is about 15 meV, which is significantly larger than the small spacing (of about 3 meV) in the rigid lattice indicating a much stronger spatial confinement. This is a direct consequence of the additional strain potentials in the reconstructed lattice. Note that also the hybridization of the higher-lying bands is strongly suppressed as there is a lack of band crossing due to their flatness in the reconstructed lattice, cf. the color gradient in Figs. 2(a) and 2(b) denoting the degree of hybridization. We need to go to higher energies to see some hybridization in the reconstructed case [red color around 10 meV in Fig. 2(a)].

The moiré exciton wave function in real space $|\Psi(\mathbf{r})|^2$ for the lowest-lying states are shown in Figs. 2(c) and 2(d). We find that in the reconstructed lattice the wave function is localized close to the edges of the H^h_h domains of the of the moiré unit cell [cf. Fig. 2(c)], reflecting the potential minima from the strain-induced potential. In contrast, in the rigid lattice with no additional strain potential [cf. Fig. 2(d)] there is a much larger probability distribution centered at the H^h_h stacking configuration [cf. Fig. 1(b)]. Here, the moiré potential only consists of the tunneling and therefore the exciton localization is determined only by the stacking with the strongest tunneling [19]. When increasing the twist angle, the reconstructed lattice starts to revert back to the rigid lattice, making the tunneling the dominating contribution of the moiré potential. This change between different regimes implies the possibility of tuning the localization of moiré excitons, which should have important consequences for exciton transport in these materials [68,69].

IV. IMPACT OF RECONSTRUCTION ON OPTICAL SPECTRA

Having access to the moiré exciton energy landscape, we can now determine the optical response of TMD bilayers in presence of atomic reconstruction. In WSe_2 homobilayers, the lowest-lying state in R-type stacking is the strongly hybridized KΛ exciton, while in H-type stacking KΛ and K′Λ′ excitons are the lowest ones. Note that the latter two are degenerate in H-type stacking, but they have a reversed layer configuration, as a consequence of the reversed spin-orbit coupling the layers [19–21]. We first focus on PL spectra, where these dark states are expected to be visible via indirect phonon sidebands [70]. Here, the exciton can not directly emit a photon due to the large momentum mismatch between the valleys. Instead, it decays via a two-step process, first scattering to a virtual bright state within the light cone via phonon emission followed by the emission of a photon [70].

Figures 3(a) and 3(b) show the PL spectra for WSe_2 with H-type [cf. Fig. 3(a)] and R-type stacking [cf. Fig. 3(b)] at 4K at different twist angles. The reference frame for the energies are the same as in Figs. 2(a) and 2(b). We observe sidebands from momentum-dark states, where the smaller (larger) peak stems from optical (acoustic) phonon modes [19,21]. The energetic position of the KΛ(K′Λ′) phonon replicas will primarily depend on the interlayer hybridization, stemming from the strong interlayer tunneling of electrons around the Λ(Λ′) valley. This gives rise to a twist-angle-dependent dehybridization, in turn yielding a blue shift when increasing the twist angle (gray peaks in Fig. 3), i.e., the larger the twist-angle the smaller the wave function overlap [21,29]. Since this component of the moiré potential is already present in the rigid lattice we find a very similar behavior in both the rigid and the reconstructed lattice when changing the twist angle. There is, however, a clearly larger red shift for the reconstructed lattice at lower twist angles due to the

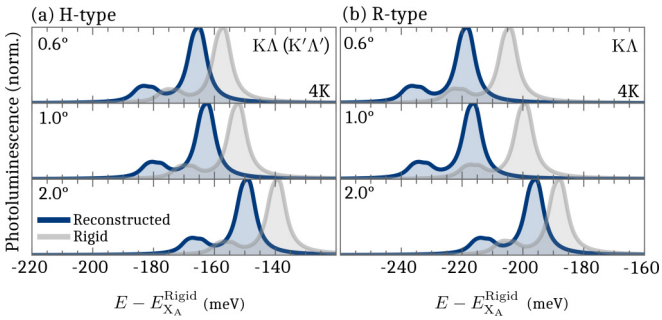

FIG. 3. Normalized photoluminescence spectrum at 4K at different twist angles, displaying phonon replicas of the energetically lowest KΛ exciton in (a) H-type and (b) R-type WSe_2 homobilyers. The spectra from the reconstructed and the rigid lattice are shown in blue and gray, respectively. A signature of lattice reconstruction is a more pronounced red shift of the exciton resonance for smaller twist angles.

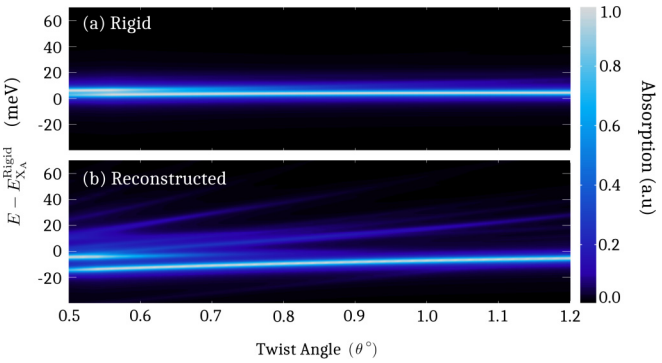

FIG. 4. Twist-angle dependence of the normalized absorption in H-type WSe_2 bilayers for (a) the rigid lattice and (b) the reconstructed lattice. The emergence of multiple peaks in the latter is due to the strain-induced intralayer potential and is an unambiguous signature of lattice reconstruction.

increasing strain-induced potentials. This is especially noticeable for R-type stacking where the piezo potential contributes to the effective exciton potential. Consequently, the change in the peak position closely resembles the change in the effective exciton potential for KΛ (Fig. S3 in the SM [48]). In Fig. 3(b) we can also see that the peak position of the reconstructed lattice is converging toward the peak position of the rigid lattice when increasing the twist angle, indicating that the lattice becomes more rigid at larger angles. So far we have been focusing on photoluminescence that is dominated by phonon sidebands of the energetically lowest dark KΛ excitons. These states are strongly hybridized [19,21], and are thus subject to a pronounced moiré potential already in the rigid lattice. The situation is qualitatively different for bright KK excitons that are accessible in absorption spectra. Here, the reconstructed lattice gives rise to a deep strain-induced potential, whereas the rigid lattice only experiences a small moiré potential due to the weak periodic tunneling strength around the K valley. In Fig. 2(a) we have already demonstrated the significant change occurring in the band structure of KK excitons, where multiple flat-bands have emerged in the reconstructed lattice for both the intralayer and the interlayer excitons.

In Figs. 4(a) and 4(b), we have calculated the absorption spectrum of H-type stacked WSe_2 bilayers as a continuous function of the twist angle for both the rigid lattice [Fig. 4(a)] and the reconstructed lattice [Fig. 4(b)]. Here, we immediately observe a drastic change in the spectrum, where below $\theta \approx 1.0^\circ$ multiple peaks appear in a reconstructed lattice—in stark contrast to the single-peak spectra in the rigid lattice that are mostly angle independent. Furthermore, at smaller angles we find a noticeable splitting around ∼15 meV between the two brightest peaks in the reconstructed lattice—in good agreement with experimental observations [44]. We also find a small splitting in the rigid lattice due to the tunneling of holes, which consequently traps the lowest state at H^h_h [cf. Fig. 2(d)]. This state, however, is very close to the next nontrapped state [cf. Fig. 2(b)], and thus the trapping is not very efficient. In the reconstructed lattice [cf. Fig. 4(b)], we instead have a rich optical response, consisting of multiple peaks. Here, the lowest branches stem from excitons trapped in the deep strain potential pockets [cf. Figs. 2(a) and 2(c). Consequently, these peaks undergo a nonlinear blue shift as we increase the twist angle, following the nonlinear twist angle dependence of the strain-induced moiré potential [cf. Fig. 1(g)]. Furthermore, in Fig. 2(a), we find that the lowest lying KK states are of pure interlayer character [black lines in Fig. 2(a)]. These are not visible in absorption spectra due to their orders of magnitude smaller overlap between the electron and the hole wave function compared to intralayer excitons [71]. When increasing the twist angle, the number of peaks is reduced until it converges to the rigid lattice case around $\theta = 1.2^\circ$ that is characterized by only one resonance.

In R-type stacking (shown in the SM [48]), we do not observe the same effect. Here, the strain-induced potential for intralayer KK excitons is negligible and the impact on the spectra only stems from the weak tunneling of carriers. We predict this drastic change in optical absorption due to atomic reconstruction to be similar for all naturally stacked TMD homobilayers. Note that the multipeak structure is also well known from TMD heterostructures, such as $MoSe_2 - WSe_2$, already in the rigid lattice case due to deep moiré potentials [30]. Here, the impact of lattice reconstruction is only of quantitative nature with changes for the peak separation and amplitude. The situation is qualitatively different in naturally stacked TMD homobilayers, where the strain-induced potential in the reconstructed lattice is the dominant mechanism and leads to the characteristic multi-peak structure for the bright A exciton. The latter can thus be considered as an unambiguous optical signature for the presence of lattice reconstruction.

V. CONCLUSION

Overall, our work provides microscopic insights into many-particle mechanisms dominating the optical response in twisted TMD homobilayers. The atomic reconstruction has a large impact on the moiré exciton energy landscape where strain-induced potentials lead to significant red shifts and multiple new flat bands. Furthermore, we have calculated moiré exciton wave functions and predict that excitons are trapped at different sites in the reconstructed lattice reflecting the maxima of the strain potentials. Finally, we find a significant

change in optical spectra of naturally stacked TMD homobilayers due to reconstruction. In particular, we predict the emergence of a multipeak structure in absorption spectra—in stark contrast to the single-peak dominated spectra in a rigid lattice. Our work can help guide future experiments in the growing field of 2D material twistronics.

ACKNOWLEDGMENTS

We thank M. Feierabend for insightful discussions. This project has received funding from Deutsche Forschungsgemeinschaft via CRC 1083 (Project No. B09) and the regular Project No. 512604469.

[1] P. Ares and K. S. Novoselov, Recent advances in graphene and other 2d materials, Nano Mater. Sci. **4**, 3 (2022).

[2] A. Ciarrocchi, F. Tagarelli, A. Avsar, and A. Kis, Excitonic devices with van der Waals heterostructures: Valleytronics meets twistronics, Nat. Rev. Mater. **7**, 449 (2022).

[3] E. Y. Andrei and A. H. MacDonald, Graphene bilayers with a twist, Nat. Mater. **19**, 1265 (2020).

[4] Q. Tong, H. Yu, Q. Zhu, Y. Wang, X. Xu, and W. Yao, Topological mosaics in moiré superlattices of van der Waals heterobilayers, Nat. Phys. **13**, 356 (2017).

[5] Y. Cao, V. Fatemi, S. Fang, K. Watanabe, T. Taniguchi, E. Kaxiras, and P. Jarillo-Herrero, Unconventional superconductivity in magic-angle graphene superlattices, Nature (London) **556**, 43 (2018).

[6] L. Wang, E.-M. Shih, A. Ghiotto, L. Xian, D. A. Rhodes, C. Tan, M. Claassen, D. M. Kennes, Y. Bai, B. Kim, K. Watanabe, T. Taniguchi, X. Zhu, J. Hone, A. Rubio, A. N. Pasupathy, and C. R. Dean, Correlated electronic phases in twisted bilayer transition metal dichalcogenides, Nat. Mater. **19**, 861 (2020).

[7] A. K. Geim and I. V. Grigorieva, Van der Waals heterostructures, Nature (London) **499**, 419 (2013).

[8] W. Liao, Y. Huang, H. Wang, and H. Zhang, van der Waals heterostructures for optoelectronics: Progress and prospects, Appl. Mater. Today **16**, 435 (2019).

[9] R. Perea-Causin, D. Erkensten, J. M. Fitzgerald, J. J. Thompson, R. Rosati, S. Brem, and E. Malic, Exciton optics, dynamics, and transport in atomically thin semiconductors, APL Mater. **10**, 100701 (2022).

[10] D. Schmitt, J. P. Bange, W. Bennecke, A. AlMutairi, G. Meneghini, K. Watanabe, T. Taniguchi, D. Steil, D. R. Luke, R. T. Weitz, S. Steil, G. S. M. Jansen, S. Brem, E. Malic, S. Hofmann, M. Reutzel, and S. Mathias, Formation of moiré interlayer excitons in space and time, Nature (London) **608**, 499 (2022).

[11] T. Mueller and E. Malic, Exciton physics and device application of two-dimensional transition metal dichalcogenide semiconductors, npj 2D Mater. Appl. **2**, 29 (2018).

[12] A. Splendiani, L. Sun, Y. Zhang, T. Li, J. Kim, C.-Y. Chim, G. Galli, and F. Wang, Emerging photoluminescence in monolayer MoS_2, Nano Lett. **10**, 1271 (2010).

[13] Z. Wang, Y.-H. Chiu, K. Honz, K. F. Mak, and J. Shan, Electrical tuning of interlayer exciton gases in WSe_2 bilayers, Nano Lett. **18**, 137 (2018).

[14] M. M. Altaiary, E. Liu, C.-T. Liang, F.-C. Hsiao, J. van Baren, T. Taniguchi, K. Watanabe, N. M. Gabor, Y.-C. Chang, and C. H. Lui, Electrically switchable intervalley excitons with strong two-phonon scattering in bilayer WSe_2, Nano Lett. **22**, 1829 (2022).

[15] Z. Huang, Y. Zhao, T. Bo, Y. Chu, J. Tian, L. Liu, Y. Yuan, F. Wu, J. Zhao, L. Xian, K. Watanabe, T. Taniguchi, R. Yang, D. Shi, L. Du, Z. Sun, S. Meng, W. Yang, and G. Zhang, Spatially indirect intervalley excitons in bilayer WSe_2, Phys. Rev. B **105**, L041409 (2022).

[16] P. Rivera, J. R. Schaibley, A. M. Jones, J. S. Ross, S. Wu, G. Aivazian, P. Klement, K. Seyler, G. Clark, N. J. Ghimire, J. Yan, D. G. Mandrus, W. Yao, and X. Xu, Observation of long-lived interlayer excitons in monolayer $MoSe_2$–WSe_2 heterostructures, Nat. Commun. **6**, 6242 (2015).

[17] B. Miller, A. Steinhoff, B. Pano, J. Klein, F. Jahnke, A. Holleitner, and U. Wurstbauer, Long-lived direct and indirect interlayer excitons in van der Waals heterostructures, Nano Lett. **17**, 5229 (2017).

[18] J. Kunstmann, F. Mooshammer, P. Nagler, A. Chaves, F. Stein, N. Paradiso, G. Plechinger, C. Strunk, C. Schüller, G. Seifert, D. R. Reichman, and T. Korn, Momentum-space indirect interlayer excitons in transition-metal dichalcogenide van der Waals heterostructures, Nat. Phys. **14**, 801 (2018).

[19] J. Hagel, S. Brem, C. Linderälv, P. Erhart, and E. Malic, Exciton landscape in van der Waals heterostructures, Phys. Rev. Res. **3**, 043217 (2021).

[20] F. Tagarelli, E. Lopriore, D. Erkensten, R. Perea-Causín, S. Brem, J. Hagel, Z. Sun, G. Pasquale, K. Watanabe, T. Taniguchi, E. Malic, and A. Kis, Electrical control of hybrid exciton transport in a van der Waals heterostructure, Nat. Photon. **17**, 615 (2023).

[21] S. Brem, K.-Q. Lin, R. Gillen, J. M. Bauer, J. Maultzsch, J. M. Lupton, and E. Malic, Hybridized intervalley moiré excitons and flat bands in twisted WSe_2 bilayers, Nanoscale **12**, 11088 (2020).

[22] I. C. Gerber, E. Courtade, S. Shree, C. Robert, T. Taniguchi, K. Watanabe, A. Balocchi, P. Renucci, D. Lagarde, X. Marie, and B. Urbaszek, Interlayer excitons in bilayer MoS_2 with strong oscillator strength up to room temperature, Phys. Rev. B **99**, 035443 (2019).

[23] E. M. Alexeev, D. A. Ruiz-Tijerina, M. Danovich, M. J. Hamer, D. J. Terry, P. K. Nayak, S. Ahn, S. Pak, J. Lee, J. I. Sohn, M. R. Molas, M. Koperski, K. Watanabe, T. Taniguchi, K. S. Novoselov, R. V. Gorbachev, H. S. Shin, V. I. Falko, and A. I. Tartakovskii, Resonantly hybridized excitons in moiré superlattices in van der Waals heterostructures, Nature (London) **567**, 81 (2019).

[24] G. Meneghini, S. Brem, and E. Malic, Ultrafast phonon-driven charge transfer in van der Waals heterostructures, Nat. Sci. **2**, e20220014 (2022).

[25] K. L. Seyler, P. Rivera, H. Yu, N. P. Wilson, E. L. Ray, D. G. Mandrus, J. Yan, W. Yao, and X. Xu, Signatures of moiré-trapped valley excitons in $MoSe_2$/WSe_2 heterobilayers, Nature (London) **567**, 66 (2019).

[26] K. Tran, G. Moody, F. Wu, X. Lu, J. Choi, K. Kim, A. Rai, D. A. Sanchez, J. Quan, A. Singh, J. Embley, A. Zepeda, M.

Campbell, T. Autry, T. Taniguchi, K. Watanabe, N. Lu, S. K. Banerjee, K. L. Silverman, S. Kim *et al.*, Evidence for moiré excitons in van der Waals heterostructures, Nature (London) **567**, 71 (2019).

[27] Q. Tong, M. Chen, F. Xiao, H. Yu, and W. Yao, Interferences of electrostatic moiré potentials and bichromatic superlattices of electrons and excitons in transition metal dichalcogenides, 2D Mater. **8**, 025007 (2021).

[28] H. Yu, G.-B. Liu, J. Tang, X. Xu, and W. Yao, Moiré excitons: From programmable quantum emitter arrays to spin-orbit–coupled artificial lattices, Sci. Adv. **3**, e1701696 (2017).

[29] P. Merkl, F. Mooshammer, S. Brem, A. Girnghuber, K.-Q. Lin, L. Weigl, M. Liebich, C.-K. Yong, R. Gillen, J. Maultzsch, J. M. Lupton, E. Malic, and R. Huber, Twist-tailoring coulomb correlations in van der Waals homobilayers, Nat. Commun. **11**, 2167 (2020).

[30] S. Brem, C. Linderälv, P. Erhart, and E. Malic, Tunable phases of moiré excitons in van der Waals heterostructures, Nano Lett. **20**, 8534 (2020).

[31] J. Hagel, S. Brem, and E. Malic, Electrical tuning of moiré excitons in $MoSe_2$ bilayers, 2D Mater. **10**, 014013 (2023).

[32] J. Choi, M. Florian, A. Steinhoff, D. Erben, K. Tran, D. S. Kim, L. Sun, J. Quan, R. Claassen, S. Majumder, J. A. Hollingsworth, T. Taniguchi, K. Watanabe, K. Ueno, A. Singh, G. Moody, F. Jahnke, and X. Li, Twist angle-dependent interlayer exciton lifetimes in van der Waals heterostructures, Phys. Rev. Lett. **126**, 047401 (2021).

[33] M. Förg, A. S. Baimuratov, S. Y. Kruchinin, I. A. Vovk, J. Scherzer, J. Förste, V. Funk, K. Watanabe, T. Taniguchi, and A. Högele, Moiré excitons in $MoSe_2$-WSe_2 heterobilayers and heterotrilayers, Nat. Commun. **12**, 1656 (2021).

[34] C. Jin, E. C. Regan, A. Yan, M. I. B. Utama, D. Wang, S. Zhao, Y. Qin, S. Yang, Z. Zheng, S. Shi, K. Watanabe, T. Taniguchi, S. Tongay, A. Zettl, and F. Wang, Observation of moiré excitons in WSe_2/WS_2 heterostructure superlattices, Nature (London) **567**, 76 (2019).

[35] A. Weston, Y. Zou, V. Enaldiev, A. Summerfield, N. Clark, V. Zólyomi, A. Graham, C. Yelgel, S. Magorrian, M. Zhou, J. Zultak, D. Hopkinson, A. Barinov, T. H. Bointon, A. Kretinin, N. R. Wilson, P. H. Beton, V. I. Falko, S. J. Haigh, and R. Gorbachev, Atomic reconstruction in twisted bilayers of transition metal dichalcogenides, Nat. Nanotechnol. **15**, 592 (2020).

[36] M. R. Rosenberger, H.-J. Chuang, M. Phillips, V. P. Oleshko, K. M. McCreary, S. V. Sivaram, C. S. Hellberg, and B. T. Jonker, Twist angle-dependent atomic reconstruction and moiré patterns in transition metal dichalcogenide heterostructures, ACS Nano **14**, 4550 (2020).

[37] M. Van Winkle, I. M. Craig, S. Carr, M. Dandu, K. C. Bustillo, J. Ciston, C. Ophus, T. Taniguchi, K. Watanabe, A. Raja, S. M. Griffin, and D. K. Bediako, Rotational and dilational reconstruction in transition metal dichalcogenide moiré bilayers, Nat. Commun. **14**, 2989 (2023).

[38] M. H. Naik, E. C. Regan, Z. Zhang, Y.-H. Chan, Z. Li, D. Wang, Y. Yoon, C. S. Ong, W. Zhao, S. Zhao, M. I. B. Utama, B. Gao, X. Wei, M. Sayyad, K. Yumigeta, K. Watanabe, T. Taniguchi, S. Tongay, F. H. da Jornada, F. Wang *et al.*, Intralayer charge-transfer moiré excitons in van der Waals superlattices, Nature (London) **609**, 52 (2022).

[39] H. Li, S. Li, M. H. Naik, J. Xie, X. Li, J. Wang, E. Regan, D. Wang, W. Zhao, S. Zhao, S. Kahn, K. Yumigeta, M. Blei, T. Taniguchi, K. Watanabe, S. Tongay, A. Zettl, S. G. Louie, F. Wang, and M. F. Crommie, Imaging moiré flat bands in three-dimensional reconstructed WSe_2/WS_2 superlattices, Nat. Mater. **20**, 945 (2021).

[40] C. Zhang, C.-P. Chuu, X. Ren, M.-Y. Li, L.-J. Li, C. Jin, M.-Y. Chou, and C.-K. Shih, Interlayer couplings, moiré patterns, and 2d electronic superlattices in MoS_2/WSe_2 hetero-bilayers, Sci. Adv. **3**, e1601459 (2017).

[41] S. Zhao, Z. Li, X. Huang, A. Rupp, J. Göser, I. A. Vovk, S. Y. Kruchinin, K. Watanabe, T. Taniguchi, I. Bilgin, A. S. Baimuratov, and A. Högele, Excitons in mesoscopically reconstructed moiré heterostructures, Nat. Nanotechnol. **18**, 572 (2023).

[42] Z. Li, F. Tabataba-Vakili, S. Zhao, A. Rupp, I. Bilgin, Z. Herdegen, B. März, K. Watanabe, T. Taniguchi, G. R. Schleder, A. S. Baimuratov, E. Kaxiras, K. Müller-Caspary, and A. Högele, Lattice reconstruction in $MoSe_2$–WSe_2 heterobilayers synthesized by chemical vapor deposition, Nano Lett. **23**, 4160 (2023).

[43] J. Sung, Y. Zhou, G. Scuri, V. Zólyomi, T. I. Andersen, H. Yoo, D. S. Wild, A. Y. Joe, R. J. Gelly, H. Heo, S. J. Magorrian, D. Bérubé, A. M. M. Valdivia, T. Taniguchi, K. Watanabe, M. D. Lukin, P. Kim, V. I. Fal'ko, and H. Park, Broken mirror symmetry in excitonic response of reconstructed domains in twisted $MoSe_2/MoSe_2$ bilayers, Nat. Nanotechnol. **15**, 750 (2020).

[44] T. I. Andersen, G. Scuri, A. Sushko, K. De Greve, J. Sung, Y. Zhou, D. S. Wild, R. J. Gelly, H. Heo, D. Bérubé, A. Y. Joe, L. A. Jauregui, K. Watanabe, T. Taniguchi, P. Kim, H. Park, and M. D. Lukin, Excitons in a reconstructed moiré potential in twisted WSe_2/WSe_2 homobilayers, Nat. Mater. **20**, 480 (2021).

[45] V. V. Enaldiev, V. Zólyomi, C. Yelgel, S. J. Magorrian, and V. I. Fal'ko, Stacking domains and dislocation networks in marginally twisted bilayers of transition metal dichalcogenides, Phys. Rev. Lett. **124**, 206101 (2020).

[46] S. Carr, D. Massatt, S. B. Torrisi, P. Cazeaux, M. Luskin, and E. Kaxiras, Relaxation and domain formation in incommensurate two-dimensional heterostructures, Phys. Rev. B **98**, 224102 (2018).

[47] F. Ferreira, S. Magorrian, V. Enaldiev, D. Ruiz-Tijerina, and V. Fal'ko, Band energy landscapes in twisted homobilayers of transition metal dichalcogenides, Appl. Phys. Lett. **118**, 241602 (2021).

[48] See Supplemental Material at http://link.aps.org/supplemental/10.1103/PhysRevMaterials.8.034001 for further results and details concerning the theoretical model, which also includes Refs. [49–57].

[49] K.-A. N. Duerloo, M. T. Ong, and E. J. Reed, Intrinsic piezoelectricity in two-dimensional materials, J. Phys. Chem. Lett. **3**, 2871 (2012).

[50] H. Rostami, F. Guinea, M. Polini, and R. Roldán, Piezoelectricity and valley chern number in inhomogeneous hexagonal 2d crystals, npj 2D Mater. Appl. **2**, 15 (2018).

[51] F. Bernardini, V. Fiorentini, and D. Vanderbilt, Spontaneous polarization and piezoelectric constants of III-V nitrides, Phys. Rev. B **56**, R10024 (1997).

[52] E. Cappelluti, R. Roldán, J. A. Silva-Guillén, P. Ordejón, and F. Guinea, Tight-binding model and direct-gap/indirect-gap transition in single-layer and multilayer MoS_2, Phys. Rev. B **88**, 075409 (2013).

[53] H. Rostami, R. Roldán, E. Cappelluti, R. Asgari, and F. Guinea, Theory of strain in single-layer transition metal dichalcogenides, Phys. Rev. B **92**, 195402 (2015).

[54] D. A. Ruiz-Tijerina and V. I. Fal'ko, Interlayer hybridization and moiré superlattice minibands for electrons and excitons in heterobilayers of transition-metal dichalcogenides, Phys. Rev. B **99**, 125424 (2019).

[55] F. Katsch, M. Selig, A. Carmele, and A. Knorr, Theory of exciton–exciton interactions in monolayer transition metal dichalcogenides, Phys. Status Solidi (b) **255**, 1800185 (2018).

[56] A. Laturia, M. L. Van de Put, and W. G. Vandenberghe, Dielectric properties of hexagonal boron nitride and transition metal dichalcogenides: From monolayer to bulk, npj 2D Mater. Appl. **2**, 6 (2018).

[57] L. D. Landau, E. M. Lifshitz, A. M. Kosevich, and L. P. Pitaevskii, *Theory of Elasticity: Volume 7* (Elsevier, Amsterdam, Netherlands, 1986).

[58] C. Linderälv, J. Hagel, S. Brem, E. Malic, and P. Erhart, The moiré potential in twisted transition metal dichalcogenide bilayers arXiv:2205.15616.

[59] B. Amorim, A. Cortijo, F. De Juan, A. G. Grushin, F. Guinea, A. Gutiérrez-Rubio, H. Ochoa, V. Parente, R. Roldán, P. San-Jose, J. Schiefele, M. Sturla, and M. A. H. Vozmediano, Novel effects of strains in graphene and other two dimensional materials, Phys. Rep. **617**, 1 (2016).

[60] M. A. Cazalilla, H. Ochoa, and F. Guinea, Quantum spin hall effect in two-dimensional crystals of transition-metal dichalcogenides, Phys. Rev. Lett. **113**, 077201 (2014).

[61] S. Fang, S. Carr, M. A. Cazalilla, and E. Kaxiras, Electronic structure theory of strained two-dimensional materials with hexagonal symmetry, Phys. Rev. B **98**, 075106 (2018).

[62] Z. Khatibi, M. Feierabend, M. Selig, S. Brem, C. Linderälv, P. Erhart, and E. Malic, Impact of strain on the excitonic linewidth in transition metal dichalcogenides, 2D Mater. **6**, 015015 (2018).

[63] V. Enaldiev, F. Ferreira, J. McHugh, and V. I. Fal'ko, Self-organized quantum dots in marginally twisted $MoSe_2$/WSe_2 and MoS_2/WS_2 bilayers, npj 2D Mater. Appl. **6**, 74 (2022).

[64] V. V. Enaldiev, F. Ferreira, S. J. Magorrian, and V. I. Fal'ko, Piezoelectric networks and ferroelectric domains in twistronic superlattices in WS_2/MoS_2 and WSe_2/$MoSe_2$ bilayers, 2D Mater. **8**, 025030 (2021).

[65] M. Feierabend, A. Morlet, G. Berghäuser, and E. Malic, Impact of strain on the optical fingerprint of monolayer transition-metal dichalcogenides, Phys. Rev. B **96**, 045425 (2017).

[66] S. Ovesen, S. Brem, C. Linderälv, M. Kuisma, T. Korn, P. Erhart, M. Selig, and E. Malic, Interlayer exciton dynamics in van der Waals heterostructures, Commun. Phys. **2**, 23 (2019).

[67] A. Kormányos, G. Burkard, M. Gmitra, J. Fabian, V. Zólyomi, N. D. Drummond, and V. Fal'ko, **k**·**p** theory for two-dimensional transition metal dichalcogenide semiconductors, 2D Mater. **2**, 022001 (2015).

[68] E. Malic, R. Perea-Causin, R. Rosati, D. Erkensten, and S. Brem, Exciton transport in atomically thin semiconductors, Nat. Commun. **14**, 3430 (2023).

[69] K. Wagner, J. Zipfel, R. Rosati, E. Wietek, J. D. Ziegler, S. Brem, R. Perea-Causín, T. Taniguchi, K. Watanabe, M. M. Glazov, E. Malic, and A. Chernikov, Nonclassical exciton diffusion in monolayer WSe_2, Phys. Rev. Lett. **127**, 076801 (2021).

[70] S. Brem, A. Ekman, D. Christiansen, F. Katsch, M. Selig, C. Robert, X. Marie, B. Urbaszek, A. Knorr, and E. Malic, Phonon-assisted photoluminescence from indirect excitons in monolayers of transition-metal dichalcogenides, Nano Lett. **20**, 2849 (2020).

[71] P. Merkl, F. Mooshammer, P. Steinleitner, A. Girnghuber, K.-Q. Lin, P. Nagler, J. Holler, C. Schüller, J. M. Lupton, T. Korn, S. Ovesen, S. Brem, E. Malic, and R. Huber, Ultrafast transition between exciton phases in van der Waals heterostructures, Nat. Mater. **18**, 691 (2019).